Consolidation During Drying of Aggregated Suspensions

L. A. Brown and C. F. Zukoski
Dept. of Chemical Engineering, University of Illinois at Urbana-Champaign, Urbana, IL 61801

L. R. White
Dept. of Chemical Engineering, Carnegie Mellon University, Pittsburgh, PA 15213

Drying of aqueous suspensions containing aggregated particle networks is important in a wide variety of solid/liquid unit operations where, in addition to optimizing the drying rate, there is a need for dimensional control of the dried product. During drying, the bed consolidates and then dehydrates. The degree of consolidation is sensitive to the strength of particle attractions altered by solution conditions such as pH, ionic strength, and particle size. These interaction forces are characterized in terms of an independently measurable quantity, the compressive yield stress P_y, and link P_y to the compressive capillary forces to which the suspension is subjected during drying. Using P_y and a two-phase fluid model for drying, a dimensionless parameter $\bar{Q}$ is identified to provide a guide for conditions where interparticle forces and mass-transfer limitations will dominate drying behavior. This model yields a quantitative measure of the shape changes that can be expected upon drying. Model predictions are tested using drying experiments on 0.65 μm alumina particles in aqueous suspensions at different pH and salt concentrations.

Introduction

Drying of saturated bodies involves a phase change, mass transfer, and the application of capillary stresses to the drying bodies. If the capillary forces exceed the compressive strength of the saturated body, the bed compacts and in the process expresses liquid that is carried away by evaporation. Under these conditions, drying is controlled by the relative rates of mass transfer and the ease with which the bed collapses to allow the surface to remain saturated. In the limit of slow evaporation or rapid bed collapse, variations in volume fraction within the drying body are minimized. However, at the opposite extreme of rapid evaporation or slow bed collapse, large volume fraction gradients are generated and the slurry may develop a crust. The ease of collapse is controlled by the microstructure of the bed and the strength of interparticle bonds. As a result, incorporation of interparticle forces into descriptions of drying is an essential step to developing useful models for controlling both drying rates and dimensional stability of the drying body.

Correspondence concerning this article should be addressed to C. F. Zukoski.

Traditional approaches treat drying of compressible slurries as the consolidation of a viscoelastic body (Scherer, 1990; Smith et al., 1995). The goal of these models is to determine the rates of drying that are commonly broken into an initial constant rate period followed by one or more falling rate periods. Application of these models is not straightforward due to difficulties in estimating parameters used in the viscoelastic constitutive equation such as Poisson's ratio, the elastic modulus, and the viscosity. We develop here a model of slurry drying that incorporates the strengths of interparticle bonds through the compressive yield stress of the suspension P_y and the volume fraction-dependent permeability. The permeability can be estimated with standard models (Landman and White, 1992), while P_y can be measured independently over the entire volume fraction range of interest (Miller et al., 1996; Green, 1997). This approach simplifies linking model predictions to particle and bed properties.

Our model is based on a two-phase fluid description of the suspension developed and extensively tested in descriptions of pressure filtration (Landman et al., 1991). We adopt these

descriptions to drying by recognizing that, at the onset of drying, capillary forces at the slurry gas interface exert a compressive force on the slurry. The bed will collapse as long as the slurry collapses more easily than the evaporated liquid can move away from the interface. However, as the bed collapses, its resistance to compaction grows. At a certain point, P_y at the surface equals the capillary stresses and gas enters the drying body (that is, the body begins to desaturate). Our model describes the drying process up to this desaturation point. However, as discussed below, under many circumstances the model captures not only the initial drying of the bed, but also provides good estimates of the time to completely dry (that is, desaturate) the body.

In the next section a description is developed of the drying of saturated compressible beds. During this time period, continuous loss of solvent occurs at the expense of shrinkage of the saturated body. The model developed in the next section describes consolidation up to the point at which the bed starts to desaturate. To demonstrate the relative importance of interparticle forces, a series of calculations are made based on systems where model input parameters have been experimentally verified. These calculations show that by changing interparticle forces and drying rates, substantial differences in shrinkage and in volume fraction gradients can be produced. The model can be used to estimate the time required for the bed to start desaturating and the amount of liquid left in the bed at that time. In the section Model Inputs, the experimental system is described from which the input parameters for the model are determined. The following section presents model predictions and experimental comparisons. Conclusions are drawn in the final section.

Model Development

The consolidation of colloidal suspensions during filtration and sedimentation has been studied extensively (Kynch, 1952; Tiller, 1981; Fitch, 1983; Buscall and White, 1987). Here, we follow the treatment of Landman et al. (1991) in their study of pressure filtration. As the drying process involves a phase change and thus possible temperature changes in the drying body with time, we also incorporate the appropriate equations to describe heat transfer within the drying body and the impact of temperature changes on the rate of drying.

In the language standard to descriptions of drying (Sherwood, 1929a, b, 1930), the consolidation model covers only the initial transient and constant rate periods of drying. There is a change in the mechanism that controls drying rate behavior as the solid volume fraction at the gas/bed interface approaches the value ϕ_e, where the compressive yield stress of the network equals the capillary forces. When this occurs, only the portions of the bed with volume fraction less than ϕ_e continue to consolidate. At this point, the rate controlling mechanism becomes the movement of vapor through the consolidated bed.

Consolidation model

The consolidation model considers the drying body to comprise two phases on which forces are balanced: a particulate phase of pressure P_s and velocity u, and a fluid phase of pressure P_l and velocity v. We emphasize here that $P_s(P_l)$ is the force on the solid (liquid) phase per unit total area of solid and liquid. The fluid and solid velocities are determined as the volume flux of solid or liquid per unit area of suspension. The body is bounded at least partially by a gaseous interface. The liquid evaporates into this gaseous phase and is transferred away from the drying body by diffusion or convection. While the model is readily generalized for complex geometries, we focus here on a one-dimensional drying problem to emphasize the underlying processes. Force balances are carried out on the drying body neglecting gravitational effects and assuming shear stresses are small relative to the compressive yield stresses. As detailed in the derivation in Appendix A, these force balances result in equations with two terms for each phase.

For the particulate phase

$$\frac{\partial P_s}{\partial z} + \frac{\eta R(\phi)}{a_p^2}(u - v) = 0 \tag{1}$$

For the fluid phase

$$\frac{\partial P_l}{\partial z} + \frac{\eta R(\phi)}{a_p^2}(v - u) = 0 \tag{2}$$

P_s is explicitly defined in these equations as the stress between particles arising from interparticle (colloidal) or contact forces. It is the force acting on the particles per unit suspension area. The pressure in the liquid phase P_l is the standard liquid pressure and thus is the force acting on the liquid per unit area of the liquid. The force balances are coupled through the hydrodynamic drag that develops due to differences in the continuous phase and solid phase velocities v and u in the z-direction, respectively. The force per unit volume per unit velocity due to differences between the fluid and solid velocity is

$$\frac{\eta R(\phi)}{a_p^2} \tag{3}$$

where η is the liquid viscosity, a_p is the particle radius, and ϕ is the volume fraction of solids. The term $R(\phi)$ accounts for volume fraction dependence of the drag. We choose it to have a form

$$R(\phi) = \frac{C\phi}{(1-\phi)^n} \tag{4}$$

which provides an excellent fit to experimental data. Methods developed for the experimental determination of n for aggregated suspensions are well documented (Landman and White, 1992, 1994; Landman et al., 1995). Buscall et al. (1982) and Kops-Werkhoven and Fijnant (1982) determined that the value of n for uniform hard spheres lay between 5.0 and 6.7. The constant C will be a function of particle shape and size distribution. For a monodisperse system of spherical particles, $C = 4.5$.

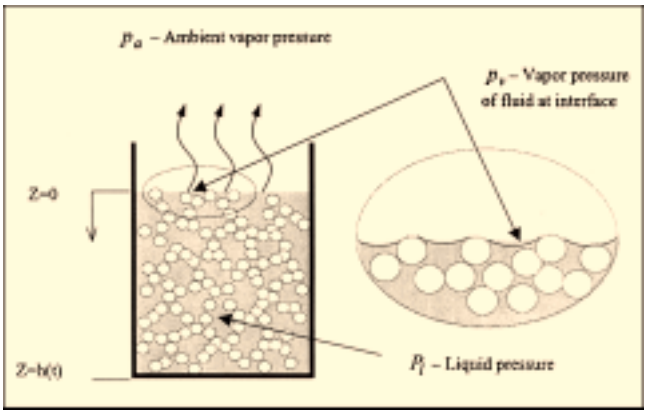

Figure 1. Saturated drying system.

The equations of continuity for these aggregated suspensions may be written as

$$\frac{\partial \phi}{\partial t} + \frac{\partial (\phi u)}{\partial z} = 0 \tag{5}$$

$$\frac{\partial (1-\phi)}{\partial t} + \frac{\partial [(1-\phi)v]}{\partial z} = 0 \tag{6}$$

Adding Eqs. 5 and 6 and integrating, we obtain

$$\phi u + (1-\phi)v = k_1(t) \tag{7}$$

where $k_1(t)$ is dependent only on time.

Using the coordinate system shown in Figure 1, the applicable boundary conditions for drying are

$$\text{at } z = 0, \qquad v = -k_g(p_v - p_a) \tag{8}$$

$$\text{at } z = h(t), \qquad u = v = \frac{dh}{dt} \tag{9}$$

where the mass-transfer coefficient k_g is a function of gas velocity and system configuration, p_a is the ambient vapor pressure, p_v is the vapor pressure at the gas liquid interface, and h is the bed height (Figure 1). Equation 8 indicates that the rate of evaporation will be determined by the difference in liquid vapor pressure at the surface and the ambient vapor pressure, as well as the rate at which the air is flowing across the surface. Equation 9 shows that in the chosen frame of reference the particles and fluid at this boundary are moving at the same rate.

Following Buscall and White (1987), we treat the constitutive equation for the bed as having a form

$$\frac{D\phi}{Dt} = 0 \qquad P_s < P_y \tag{10}$$

$$\frac{D\phi}{Dt} = \kappa(\phi)\left[P_s - P_y\right] \qquad P_s \geq P_y \tag{11}$$

where $\kappa(\phi)$ is the dynamic compressibility, P_s is the particle network stress, and P_y is the compressive yield stress. Equations 10 and 11 indicate that the network behaves plastically for $P_s > P_y$ and, using Equations 5 and 6, we can replace them with

$$\frac{\partial u}{\partial z} = 0 \qquad P_s < P_y \tag{12}$$

$$\frac{\partial u}{\partial z} = \frac{\kappa(\phi)}{\phi}\left[P_s - P_y\right] \qquad P_s \geq P_y \tag{13}$$

Buscall and White (1987) use scaling arguments to show that when $(a_p/h_0)^2 \ll 1$, where a_p is the particle radius and h_0 is the initial height of the saturated bed, $\kappa(\phi) \gg 1$, thus suggesting that $P_s - P_y \ll 1$ and allowing us to approximate P_s as $\ll$

$$P_s(z,t) = P_y(\phi(z,t)) \tag{14}$$

The link between the state of the liquid in the bed and the vapor contacting the liquid/gas interface is made by equating chemical potentials across the interface and results in the Kelvin equation

$$p_v = p_o \exp\left(\frac{P_{\text{cap}} V_m}{(R_g \theta)}\right) \tag{15}$$

where, P_{cap} is the capillary pressure at $z = 0$, p_0 is the vapor pressure that would exist above the liquid if the interface were flat, V_m is the molar volume of the liquid, R_g is the gas constant, and θ is the liquid temperature. The liquid pressure at the interface, $P_l(0,t)$ is related to the ambient pressure P_{atm} by

$$P_l(0,t) = P_{\text{atm}} + P_{\text{cap}} \tag{16}$$

Adding Eqs. 1 and 2 and integrating the resulting expression yields

$$P_{\text{atm}} = P_l(z,t) + P_s(z,t) \quad 0 \leq z \leq h(t) \tag{17}$$

)If we substitute for $P_l(0,t)$ in Eq. 16 from Eq. 17, we obtain a relationship of the form

$$P_s(0,t) = -P_{\text{cap}}[\phi(0,t)] \tag{18}$$

Equation 18 can be rewritten using Eq. 14 as

$$P_y[\phi(0,t)] = -P_{\text{cap}}[\phi(0,t)] \tag{19}$$

Inserting this expression into Eq. 15 yields

$$p_v = p_0 \exp\left\{-\frac{P_y[\phi(0,t)]V_m}{R_g \theta}\right\} \tag{20}$$

Equation 20 shows that the vapor pressure above the liquid interface can be affected, albeit minimally, by changes in particle network properties, thereby introducing a subtle volume fraction dependence to the rate of evaporation, as well as

explaining how changes in the interparticle forces can impact drying rate.

The capillary pressure in the liquid at the liquid/gas interface will be equivalent to the compressive yield stress of the particle network as indicated in Eq. 19. If this capillary pressure is lower than the equilibrium capillary pressure that would minimize the free energy of the system, liquid will evaporate and the capillary pressure will increase. The maximum value that this receding capillary pressure can attain occurs when the liquid at the interface is in equilibrium with the vapor phase and is given by the approximation

$$P_{\text{cap}}^{\max} = -\frac{\gamma \cos \psi_c \phi \rho_p \overline{A}_p}{(1-\phi)} \approx -\frac{3\gamma\phi}{(1-\phi)a_p} \tag{21}$$

where ψ_c is the contact angle, ρ_p is the number density of particles, and $\overline{A}_p$ is the specific surface area of the particles (White, 1982). The final expression is derived assuming that the particles are completely wet by the liquid such that $\psi_c = 0$. As long as this maximum capillary pressure exceeds the compressive yield stress at the volume fraction at the liquid/gas interface, the bed will consolidate and remain saturated.

$P_{\text{cap}}^{\max}$ will not be immediately achieved because liquid must diffuse away from the interface. The mass-transfer resistance acts to reduce the volume fraction at the interface. This phenomenon has a direct analogy in pressure filtration, where, if a load P_{applied} is applied to an aggregated bed, the volume fraction at the suspension/filter membrane is controlled by the relationship

$$P_{\text{applied}} = P_l(0,t) + P_y[\phi(0,t)] \tag{22}$$

where the suspension/membrane interface is at $z = 0$. If there is no membrane resistance, $P_l = 0$ and $P_y[\phi(0,t)] = P_{\text{applied}}$. Thus, the volume fraction at the bottom of the filter cake is found to be that where the aggregated bed can support the applied load. If, however, there is a substantial membrane resistance, the condition must be applied such that $q = R_m P_l(0,t)$ where R_m is the membrane resistance and q is the volumetric flux of liquid. The result is that the volume fraction at $z = 0$ is lower than that defined by $P_y[\phi(0,t)] = P_{\text{applied}}$. Over time, a filter cake builds up so that $P_l(0,t)$ decreases and $\phi(0,t)$ increases.

In the drying problem, the mass-transfer resistance of evaporating liquid plays the same role as R_m in pressure filtration. As the bed dries, both the capillary pressure and volume fraction increase. However, as $\phi(0,t)$ increases, more liquid is expressed such that P_{cap} is held at less than or equal to $P_{\text{cap}}^{\max}[\phi(0,t)]$. The result is that throughout the consolidation process, the mass-transfer resistance generated by the evaporating liquid plays a crucial role in controlling drying dynamics.

We define the flux of liquid from the bed as Q, where

$$Q = -\frac{dh}{dt} \tag{23}$$

By applying the boundary condition in Eq. 9 to solve for $k_1(t)$ in Eq. 7, we obtain

$$\frac{\partial P_s}{\partial z} + \frac{\eta R(\phi)}{a_p^2(1-\phi)}[u + Q] = 0 \tag{24}$$

Recognizing that at each point in the bed, the particles are at their incipient yield pressure as suggested in Eq. 15, we combine Eqs. 5 and 24 to yield

$$\frac{\partial \phi}{\partial t} = \frac{\partial}{\partial z}\left(D(\phi)\frac{\partial \phi}{\partial z} + \phi Q\right) \tag{25}$$

where

$$D(\phi) = \frac{\phi a_p^2 (1-\phi)\dfrac{dP_y}{d\phi}}{\eta R(\phi)} \tag{26}$$

This quantity $D(\phi)$ is a measure of the internal resistance to flow. Equation 25 governs the dynamics of the drying process and is solved with an initial condition given by

$$\phi(z,0) = \phi_0 \quad 0 \le z \le h_0 \tag{27}$$

The relevant boundary conditions are

$$\phi(0,t)Q + D(\phi(0,t))\left.\frac{\partial \phi}{\partial z}\right|_{(0,t)} \quad t \ge 0 \tag{28}$$

$$\left.\frac{\partial \phi}{\partial z}\right|_{(h(t),t)} = 0 \quad t \ge 0 \tag{29}$$

We simplify Eq. 25 by converting it to a fixed boundary problem using the formulation of Landman et al. (1991) and define a new variable $w(z,t)$ as

$$w(z,t) = \frac{1}{\phi_0 h_0}\int_0^z \phi(z,t)dz \qquad 0 \le w(z,t) \le 1 \tag{30}$$

We also define

$$e = \frac{(1-\phi)}{\phi} \tag{31}$$

where e is the ratio of the liquid volume to the solid volume in the saturated bed. Using these new variables, Eq. 25 is rewritten as

$$\frac{\partial e}{\partial T} = \frac{\partial}{\partial w}\left(\Delta(e)\frac{\partial e}{\partial w}\right) \tag{32}$$

with initial condition

$$e(w,0) = \frac{(1-\phi_0)}{\phi_0} \qquad 0 \le w \le 1 \tag{33}$$

and boundary conditions

$$\Delta\left[e(0,T)\right]\left.\frac{\partial e}{\partial w}\right|_{(0,T)} = \overline{Q} \qquad T \geq 0 \tag{34}$$

where

$$\Delta(e) = \frac{\phi^2 D(\phi)}{\phi_0^2 D(\phi_0)} \tag{35}$$

$$T = \frac{tD(\phi_0)}{h_0^2} \tag{36}$$

$$\overline{Q} = \frac{h_0 Q}{\phi_0 D(\phi_0)} = \frac{h_0 k_g\left[p_v(\phi_0) - p_a\right]}{\phi_0 D(\phi_0)} \tag{37}$$

The variable $\overline{Q}$ gives a quantitative measure of the rate controlling process during the consolidation phase of drying. For values of $\overline{Q} \ll 1$, evaporation of liquid at the surface of the body will limit the drying rate while higher values of $\overline{Q}$ indicate that the internal moisture movement by diffusion and capillary flow will control the drying rate. In addition, when $\overline{Q} \ll 1$, the volume fraction across the bed will be uniform. As the value of $\overline{Q}$ increases, gradients in ϕ will develop. High values of $\overline{Q}$ can be achieved by using thicker samples, by increasing the value of the evaporative mass-transfer coefficient or by increasing the vapor pressure at the surface. $\overline{Q}$ is very sensitive to ϕ_0 through $D(\phi_0)$ and, as a consequence, can be altered greatly by changes in interparticle bond strength and initial volume fraction. For example, in the next section we describe the drying of aqueous alumina suspensions composed of identical particles at the same initial volume fractions, but aggregated at different pH values. Table 1 gives values of $D(\phi_0)$ and $\overline{Q}$ for these samples at constant k_g, ϕ_0, and h_0. The values of $\overline{Q}$ indicate that for beds of 30 cm thickness, large volume fraction gradients are expected in drying the slurries at pH4, while slurries at pH9 should dry with no volume fraction gradients in the bed.

As the bed dries, the volume fraction $\phi(z,t)$ increases from the initial value of ϕ_0 until the top of the bed reaches a value ϕ_e where $P_y(\phi_e) \geq P_{\text{cap}}(\phi_e)$. Two scenarios can then follow:

(1) At high values of $\overline{Q}(\overline{Q} \gg 1)$, there are substantial volume fraction gradients in the bed. When the bed/gas interface reaches ϕ_e, the liquid recedes from the surface resulting in the formation of a "crust" or de-saturated layer at the bed surface. At this point, the bed begins to desaturate at the top, although the areas just below the top and near its base remain saturated at much lower volume fractions such that in these areas $P_y(\phi) < P_{\text{cap}}(\phi)$ and compression continues. In this region the model can still be applied provided that the mass transfer through the unsaturated portion of the bed is known. The term "crust" applied throughout this article refers to a region at the top of the drying bed, where the volume fraction is such that the particle network is strong enough to withstand the applied compressive forces without further consolidation, that is, $P_y(\phi) \geq P_{\text{cap}}(\phi)$.

(2) In the low $\overline{Q}$ regime, $(\overline{Q} \ll 1)$, where the volume fraction gradients are negligible, when the volume fraction at the top of the bed reaches ϕ_e, the remainder of the bed has volume fraction $\phi(z,t)$ such that $P_y(\phi) \geq P_{\text{cap}}(\phi)$, and the entire bed will stop consolidating and start to desaturate. Smith et al. (1995) use a different constitutive model to predict the volume fraction at which desaturation begins.

Table 1. Effects of Changes in Solution Chemistry on

Suspension	ϕ_0	h_0 (m)	$D(\phi_0)\times 10^{-8}$ (m^2/s)	$\overline{Q}$
0.65 μm Al_2O_3 pH4 0.1M NH_4Cl	0.45	0.3	9.83	1.4
0.65 μm Al_2O_3 pH9 0.1M NH_4Cl	0.45	0.3	127.79	0.11

Heat transfer

Often, the temperature changes in drying beds as a result of heat lost during evaporation and heat gained by convection from the gas being used for drying. Figure 2 illustrates the main heat flows considered during the drying process. The net effect of the heat transfer is that the temperature of the drying body will change until it reaches its wet bulb temperature where heat lost by evaporation matches heat gained by convection. Due to the sensitivity of p_v to temperature, this transient can produce substantial changes in the drying rate.

For the system configuration in Figure 1, a heat balance may be written for the suspension as

$$\frac{\partial\left(\rho_b C_{pb}\theta\right)}{\partial t} = \frac{\partial}{\partial z}\left(k_b \frac{\partial\theta}{\partial z}\right) - \frac{\partial}{\partial z}\left[\left(\rho_l C_{pl} v + \rho_s C_{ps} u\right)\theta\right] \tag{38}$$

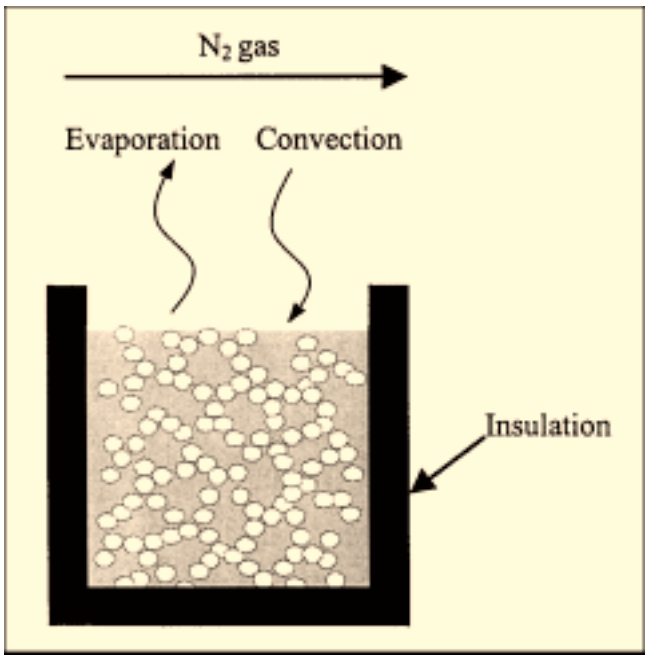

Figure 2. Heat transfer during drying of saturated system.

where θ is the temperature of the suspension at a given height z, and k_b, ρ_b, and C_{pb} are the volume averaged thermal conductivity, density, and heat capacity of the suspension, respectively. Equation 38 has the initial condition

$$\theta(z,0) = \theta_0 \tag{39}$$

and boundary conditions

$$-k\left.\frac{\partial\theta}{\partial z}\right|_{z=0} = -Q\lambda_v\rho_l + h_c\left[\theta_g - \theta(0,t)\right] \tag{40}$$

$$\left.\frac{\partial\theta}{\partial z}\right|_{z=h(t)} = 0 \tag{41}$$

where θ_g is the gas temperature, h_c is the heat-transfer coefficient, λ_v is the latent heat of vaporization, and ρ_l is the liquid density. Equation 41 indicates that the body is insulated at its base and as such there is no heat transfer from this surface. As shown in Appendix B, Eq. 38 can be rewritten using a similar approach to that used for Eq. 32.

Equation 40 may be rewritten in dimensionless form as

$$-\left.\frac{\partial\hat{\theta}}{\partial Z}\right|_{Z=0} = -\frac{Q\lambda_v\rho_l h_0}{k(\theta_0 - \theta^*_{wb})} + \frac{h_c h_0\left[\theta_g - \theta(0,t)\right]}{k(\theta_0 - \theta^*_{wb})} \tag{42}$$

where $Z = z/h_0$ and $\hat{\theta} = (\theta - \theta^*_{wb})/(\theta_0 - \theta^*_{wb})$. θ^*_{wb} is an estimate of the wet bulb temperature of the drying body obtained by solving Eq. 42 when the lefthand side is equal to zero. The actual wet bulb temperature will be different from θ^*_{wb} due to the temperature dependence of the vapor pressure and, hence, Q, as well as details of heat flux to the surface.

As shown in Eq. 42, the heat flux at the gas/liquid interface contains two dimensionless groups. The first group represents the ratio of heat lost due to evaporation to the rate of heat conduction to the surface. The second group represents the ratio of the rate of heat convection to the surface to heat conduction through the surface. When both these terms are small, heat is conducted so rapidly through the body that there are no temperature gradients in the bed. Under these conditions, Eq. 38 can be replaced by

$$\frac{dH}{dt} = h_c(\theta_g - \theta_b) - k_g\rho_l(p_v - p_a)\lambda_v \tag{43}$$

where $H = \rho_b h C_{pb}\theta_b$ and θ_b is the temperature of the body. We can make Eq. 43 dimensionless by defining

$$\hat{H} = \hat{\rho}_b\hat{h}\hat{C}_{pb}\hat{\theta} \tag{44}$$

where $\hat{\rho}_b = \rho_b/\rho_{b0}$, $\hat{h} = h/h_0$, $\hat{C}_{pb} = C_{pb}/C_{pb0}$ and $\hat{\theta}_b = (\theta_b - \theta^*_{wb})/(\theta_{g0} - \theta^*_{wb})$ where the subscript 0 refers to initial conditions and the subscript b refers to bulk or volume average conditions in the drying body.

By substituting the relevant dimensionless variables of time and temperature, we see that the heat transfer during the drying process under these conditions can be described by the differential equation

$$\frac{d\hat{H}}{dT} = c_1\left(\hat{\theta}_g - \hat{\theta}_b\right) - c_2\overline{Q} \tag{45}$$

where

$$c_1 = \frac{h_c h_0}{D(\phi_0)\rho_{b0}C_{pb0}} \tag{46}$$

and

$$c_2 = \frac{\phi_0^2\rho_l\lambda_v}{(\theta_{g0} - \theta^*_{wb})\rho_{b0}C_{pbo}} \tag{47}$$

Equation 46 has initial condition

$$\hat{H}(0) = \hat{H}_0 = \frac{(\theta_{b0} - \theta^*_{wb})}{(\theta_{g0} - \theta^*_{wb})} \tag{48}$$

Equations 32 and 38 or 45 are solved numerically for the relevant initial and boundary conditions using either the implicit finite difference method of Crank and Nicholson for Eqs. 32 and 38 or a Runge-Kutta fourth-order method for Eq. 45 (Heath, 1997).

Model Inputs

Solution of the model for volume fraction and temperature profiles in the saturated drying body as a function of time requires knowledge of several parameters. These include: the compressive yield stress P_y; the initial volume fraction ϕ_0; the mass-transfer coefficient for the system k_g; the temperature of the gas and body θ_{g0} and θ_{b0}, respectively; the initial height h_0 and diameter D of the bed, and the heat-transfer coefficient h_c. Rather than demonstrate model predictions with approximate forms of P_k, k_g, and other material properties of the suspension, we have chosen to characterize real suspensions.

Physical property data for water were obtained from standard tables (Perry and Green, 1984). Vapor pressure data for pure water was used because of the low salt concentrations. The surface tension of the solutions was measured using a "Cenco du-Nouy" tensiometer that employs the ring method (Zuidema and Waters, 1941). The Sumitomo AKP-15 0.65 μm α-Al_2O_3 particles suspended in NH_4Cl were assumed to be spherical. The heat-transfer coefficient h_c was determined using an equation proposed by (Shepherd et al., 1938) of the form

$$h_c = C_h G'^{0.8} \tag{49}$$

where C_h is a constant set equal to 14.5 and G' is the gas-flow rate across unit area of the drying surface.

As an initial test of the model, drying experiments were conducted using aqueous suspensions of commercially available Sumitomo AKP-15 1.3 μm diameter alumina particles at pH4 and pH9 and a salt concentration of 0.1 M NH_4Cl.

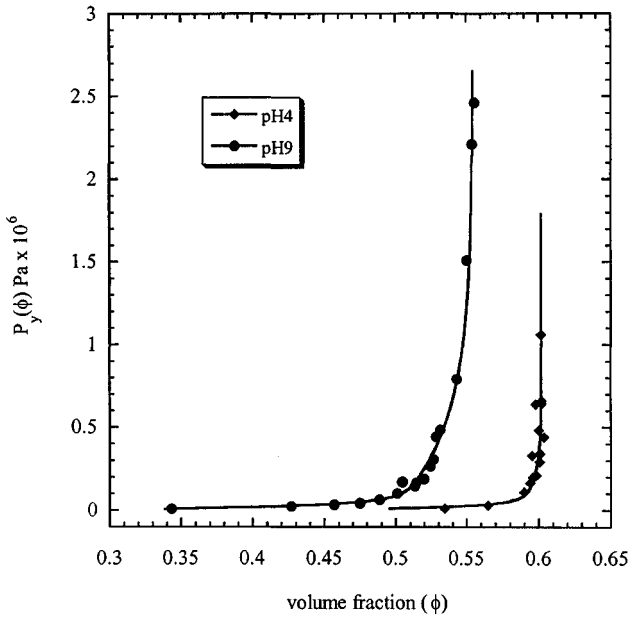

Figure 3. Compressive yield stress measurements for 0.65 μm Al_2O_3 particles at pH4 and pH9 in 0.1 M NH_4Cl, and corresponding fits using Eq. 55.

The compressive yield stress curves at pH4 and pH9 were obtained using methods outlined by Miller et al. (1996) and Green (1997). The compressive yield stress data was then fit as a function of volume fraction ϕ using a five-parameter model based on an equation developed by Garijo and Zukoski (1998) of the form

$$\phi = A_1\left(1 - A_2 \exp\left(-\frac{P_y}{A_3}\right)\right)\left(1 - A_4 \exp\left(-\frac{P_y}{A_5}\right)\right) \quad (50)$$

where the A_i are constants for a given suspension. This equation provides an excellent fit of the experimental data as shown in Figure 3. Several other three-parameter models have been employed to fit compressive yield stress data including those of Channell and Zukoski (1997) and Auzerais et al. (1988). However, these models do not accurately predict the behavior of P_y over the entire range of volume fractions. The values of the coefficients obtained from fits of P_y data using Eq. 50 are given in Table 2.

Evaporation experiments were conducted using de-ionized water to estimate the value of the mass-transfer coefficient k_g for the drying configuration used. We assumed that the same k_g value measured for de-ionized water evaporation could be used for the suspension at the corresponding height. Actual drying experiments conducted to obtain data for comparison with the simulation results involved blowing dry nitrogen gas over the samples to be dried in a fixed-bed setup with drying from one surface only. The weight changes in the samples were then recorded as a function of drying time. The temperature of the gas entering the drying cell was kept constant by passing it through a coil submerged in a heat bath to ensure entry into the drying cell at the required temperature. Due to consolidation of the sample (decreases in height), k_g was found to decrease by approximately 10% during each experiment (this was confirmed by evaporating water from the same cell and observing the effect of changing liquid height on k_g). This was accounted for in the application of the drying model.

The start of desaturation was determined from the drying curves, when the drying rate changed from being constant and was confirmed by studying video footage of the experiment which showed an elimination of glare caused by liquid at the surface at this point.

Table 2. Coefficients in Eq. 50 for 0.65 μm Al_2O_3 Particles Suspended in 0.1 M NH_4Cl at pH4 and pH9

Coefficient	pH4	pH9
A_1	0.60	0.53
A_2	1,337.7	0.106
A_3 (Pa)	989	14,427
A_4	0.104	0.634
A_5 (Pa)	58,247	106,768

Model Predictions

Solutions to Eqs. 32, 38, and 45 were determined for aqueous suspensions of 0.65 μm Al_2O_3 particles at pH4 and pH9 in 0.1 M NH_4Cl, under conditions where the mass-transfer coefficient k_g was on the order of $10^{-10} - 10^{-9}$ s·m^2·kg^{-1}. Model parameters were chosen such that $0.005 \le \overline{Q} \le 5$. Figure 3 shows the compressive yield stress curve for suspensions of 0.65 μm Al_2O_3 particles at pH4 and pH9 respectively in 0.1 M NH_4Cl salt. It can be seen from this figure that the particle network is stronger at pH9 (the particle isoelectric point) than at pH4.

Figures 4a and 4b show the drying rate behavior obtained from simulations of drying of these suspensions and the corresponding experimental results. For both simulations, $\overline{Q} \ll 1$ and consolidation is controlled by the resistance to mass transfer on the gas side. As a consequence, during consolidation in addition to the drying rates being the same, the corresponding volume fraction profiles predicted by Eq. 32 and shown in Figures 4c and 4d are quite similar. However, due to differences in strength of the particle networks, the consolidation phase ends at different volume fractions in each case. Note there are no adjustable parameters used in comparing experimental and model results in Figures 4a and 4b.

If the initial height of the saturated bed h_0 is increased while mass-transfer conditions are held constant, substantial changes in the volume fraction profiles are predicted. As shown in Figures 5 and 6, for the same sample sizes and values of k_g, the model predicts that the interparticle forces at pH4 and pH9 result in substantially different volume fraction profiles. The surface of the beds desaturates when $\phi(0,t)$ reaches ϕ_e, which is defined as the volume fraction where $P_y = P_{\text{cap}}$. For the pH4 samples, this occurs at $\phi_e = 0.597$ while for pH9 this occurs at $\phi_e = 0.526$. Note that, for pH9, $\overline{Q} < 1$ and when $\phi(0,t) = \phi_e$, the bed has a fairly uniform volume fraction profile. However, at pH4 where $\overline{Q} = 1.4$ when $\phi(0,t)$ reaches θ_e, substantial gradients exist. This phenomenon is further emphasized in Figure 7 where h_0 has been increased such that $\overline{Q} = 4.3$. Under these conditions, when $\phi(0,t)$

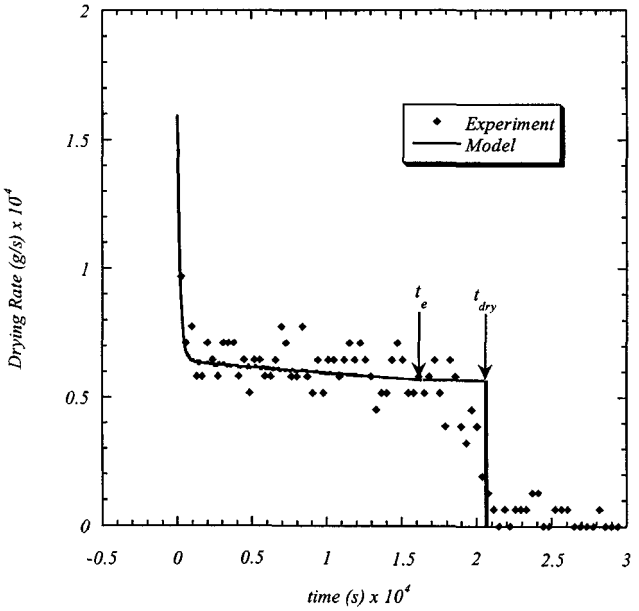

Figure 4a. Comparison of model prediction of the total drying time with experimental data for 0.65 μm Al_2O_3 particles at pH4 and 0.1 M NH_4Cl.

reaches θ_e, the volume fraction at the bottom of the bed has increased only slightly from θ_0 indicative of crusting. Figures 6 and 7 demonstrate that increasing sample size at fixed mass-transfer conditions and P_y, exacerbates crusting.

The time where the surface reaches θ_e marks the point where the bed begins to de-saturate and the falling rate period begins. For many systems where $\overline{Q} \ll 1$ and $\phi_0 \ll \phi_e$,

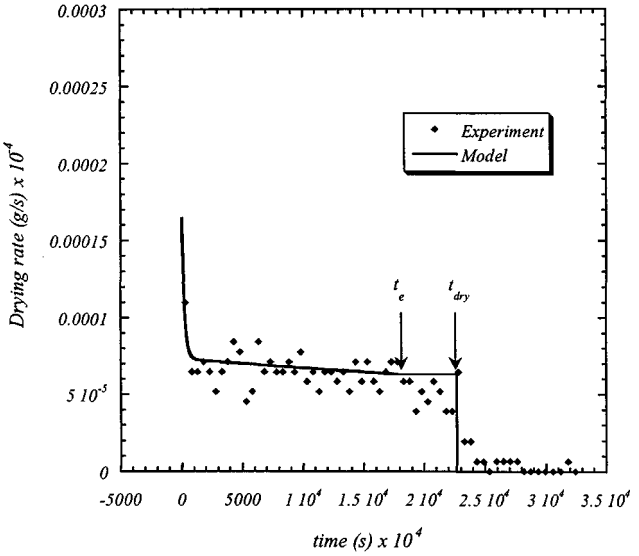

Figure 4b. Comparison of model prediction of the total drying time with experimental data for 0.65 μm Al_2O_3 particles at pH9 and 0.1 M NH_4Cl.

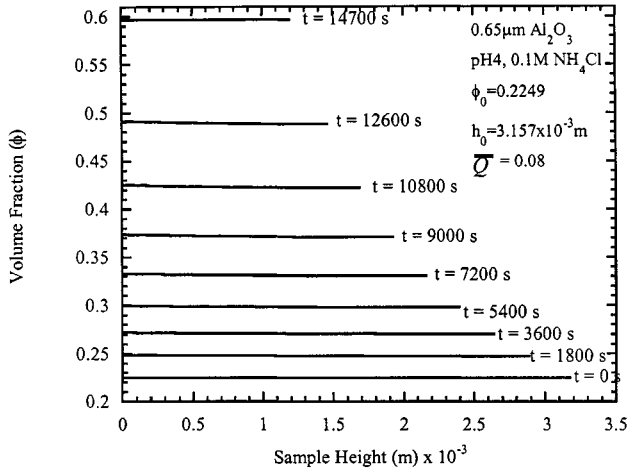

Figure 4c. Volume fraction predicted by simulation of drying of a suspension of 0.65 μm Al_2O_3 particles in 0.1 M NH_4Cl and at pH4 under conditions in Figure 4a.

the mass of liquid left in the bed at the breakthrough time t_e will be small. Under these conditions, an excellent approximation for the total drying time can be found by assuming that the rate of drying remains constant at the rate at t_e until the bed is completely de-saturated and then drops to zero. The overall drying time t_{dry} is then given by

$$t_{\text{dry}} = t_e + (1-\phi_e)\frac{h_e}{R_e} \tag{51}$$

where R_e and h_e are the rate of evaporation and the bed height respectively at t_e. This approximation is shown in Figures 4a and 4b, indicating an excellent agreement between measured and predicted drying times. As $\overline{Q}$ grows, the mass of liquid remaining in the bed at t_e will grow. As the front of

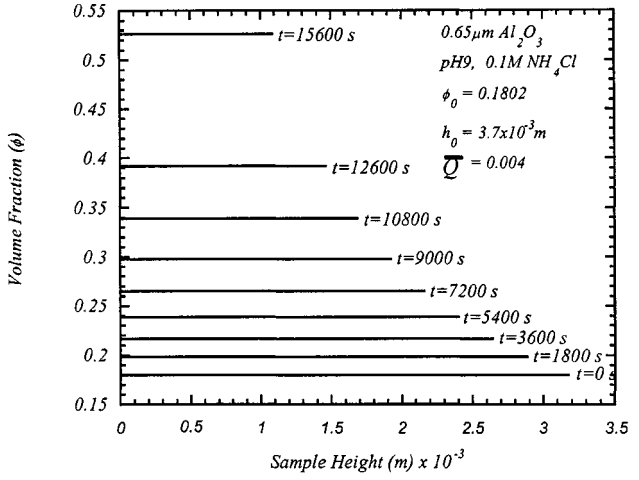

Figure 4d. Volume fraction predicted by simulation of drying of a suspension of 0.65 μm Al_2O_3 particles in 0.1 M NH_4Cl and at pH9 under conditions in Figure 4b.

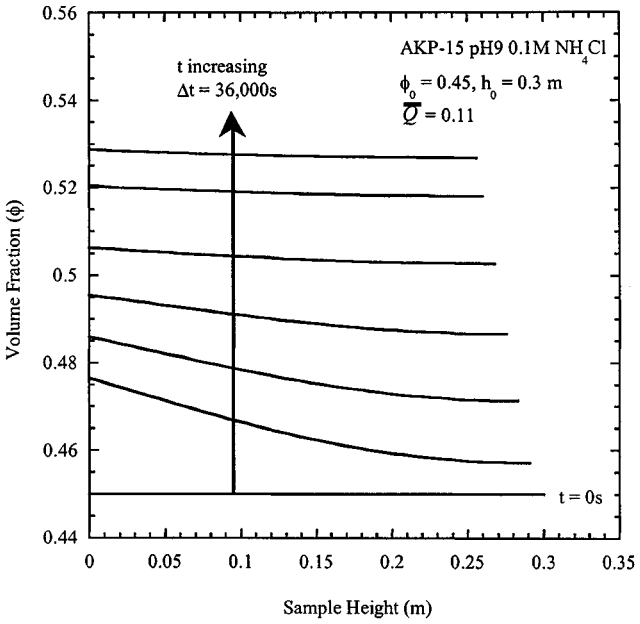

Figure 5. Volume fraction predicted as a function of drying time for 0.65 μm Al_2O_3 at pH9 and 0.1 M NH_4Cl at $\overline{Q} < 1$. Each line corresponds to a time step of 36,000 s.

liquid moves into the solid, with increasing $\overline{Q}$, we anticipate an increase in the extent of the falling rate period. In these circumstances more accurate models of drying for $t > t_e$ will be required.

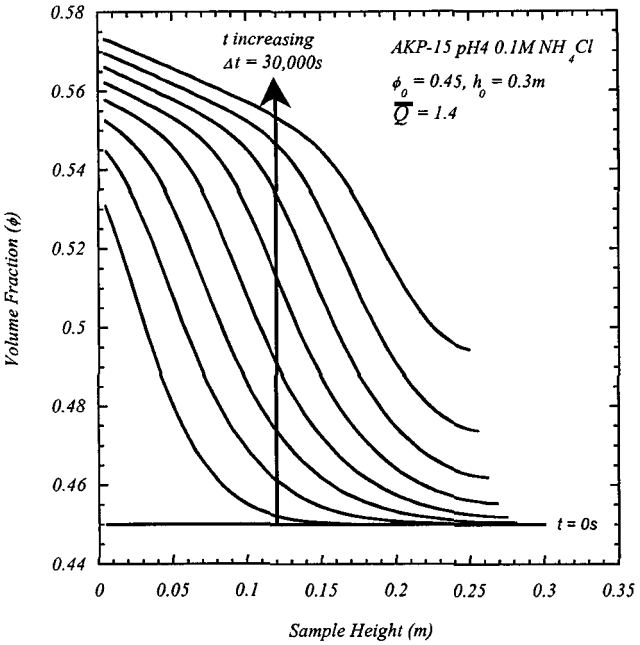

Figure 6. Volume fraction predicted as a function of drying time for 0.65 μm Al_2O_3 at pH4 and 0.1 M NH_4Cl at $\overline{Q} > 1$. Each line corresponds to a time step of 30,000 s.

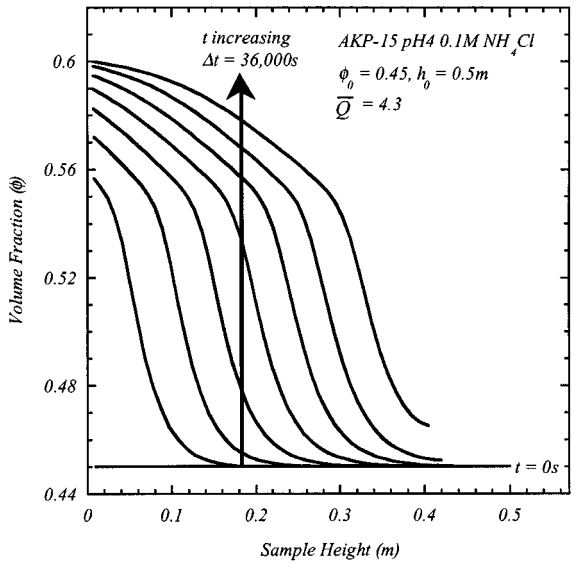

Figure 7. Volume fraction profile predicted as a function of drying time for 0.65 μm Al_2O_3 at pH9 and 0.1 M NH_4Cl at $\overline{Q} \gg 1$. Each line corresponds to a time step of 36,000 s.

Summary and Conclusions

Our model for drying of compressible beds couples the rate of mass transfer at the body/gas interface with the ability of the bed to collapse under an external load. By linking bed strength to particle properties through the compressive yield stress, we predict volume fraction variations, the cake volume fraction at which the drying front enters the drying body and the overall drying rates. For $\overline{Q} < 1$, the model captures the data very well. This is emphasized in Figures 4a and 4b where experimental results are compared with parameter-free model predictions of the drying rate.

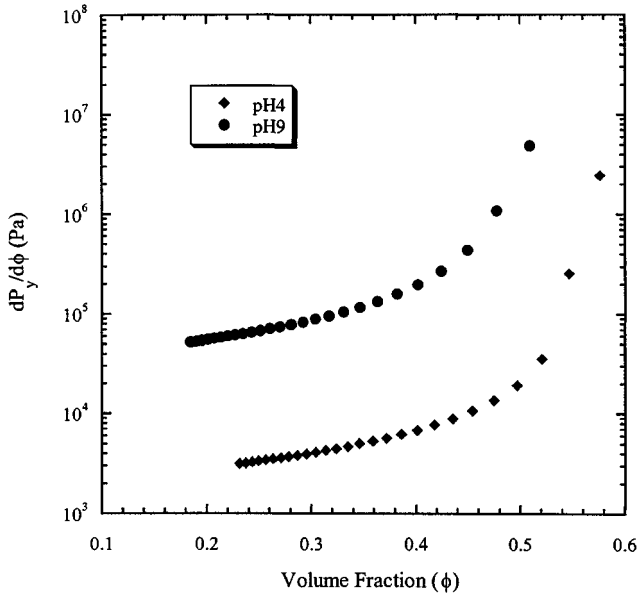

Figure 8. $dP_y/d\phi$ for 0.65 μm Al_2O_3 particles at pH4 and pH9 in 0.1 M NH_4Cl.

As discussed above, volume fraction variations in the drying body depend on the rate at which the solvent can move through the gas phase relative to the rate at which the bed can express the solvent by consolidating. The former is dominated by the mass-transfer coefficient, and thus can be controlled by the fluid mechanics of the gas phase and the geometry of the drying body. The rate at which the bed can express fluid is controlled by $dP_y/d\phi$ and the permeability of the drying cake. The strength of interparticle forces is reflected in the magnitude of P_y (Figure 8).

Under conditions where $\overline{Q} \ll 1$ (small k_g, thin cakes or weak beds), all beds will dry at a rate controlled only by the rate of mass transfer from the surface. However, the point where the drying front will enter the bed is controlled by P_y. When $\overline{Q}$ is of order unity or larger (large k_g, thick cakes or strong beds), drying rates will reflect the dynamics of bed collapse and substantial volume fraction gradients will develop in the bed.

Detailed experiments comparing model predictions with volume fractions at the termination of the consolidation stage and demonstrating the need to understand changes in P_y during the consolidation phase provide further evidence for the validity of this model. These experiments and model comparisons will be presented in a companion article.

Literature Cited

Anderson, T. B., and R. Jackson, "A Fluid Mechanical Description of Fluidized Beds," *Ind. Eng. Chem. Fund.*, **6**, 527 (1967).

Auzerais, F. M., R. Jackson, and W. B. Russel, "The Resolution of Shocks and the Effects of Compressible Sediments in Transient Settling," *J. Fluid Mech.*, **195**, 437 (1988).

Buscall, R., J. W. Goodwin, R. H. Ottewill, and Th. F. Tadros, "The Settling of Particles Through Newtonian and Non-Newtonian Media," *J. Colloid Interface Sci.*, **85**, 78 (1982).

Buscall, R., and L. R. White, "The Consolidation of Concentrated Suspensions: Part 1. The Theory of Sedimentation," *J. Chem. Soc., Faraday Trans.,1*, **83**, 873 (1987).

Channell, G. M., and C. F. Zukoski, "Shear and Compressive Rheology of Aggregated Alumina Suspensions," *AIChE J.*, **43**, 1700 (1997).

Drew, D. A., "Mathematical Modeling of Two-Phase Flow," *Ann. Rev. of Fluid Mech.*, **15**, 261 (1983).

Fitch, B., "Kynch Theory and Compression Zones," *AIChE J.*, **29**, 940 (1983).

Garijo, X., and C. F. Zukoski, personal communication, (1998).

Green, M., "Characterization of Suspensions in Settling and Compression," PhD Thesis, University of Melbourne, Australia (1997).

Heath, M. T., *Scientific Computing: An Introductory Survey,* McGraw-Hill, New York (1997).

Kops-Werkhoven, M. M., and H. M. Fijnaut, "Dynamic Behavior of Silica Dispersions Studied Near the Optical Matching Points," *J. Chem. Phys.*, **77**, 2242 (1982).

Kynch, G. J., "A Theory of Sedimentation," *Trans. Faraday Soc.*, **48**, 166 (1952).

Landman, K. A., C. Sirakoff, and L. R. White, "De-Watering of Flocculated Suspensions by Pressure Filtration," *Phys. Fluids A*, **3**, 1495 (1991).

Landman, K. A., and L. R. White, "Determination of the Hindered Settling Factor for Flocculated Suspensions," *AIChE J.*, **38**, 184 (1992).

Landman, K. A., and L. R. White, "Solid/Liquid Separation of Flocculated Suspensions," *Systems & Comput. in Japan*, **25**, 175 (1994).

Landman, K. A., L. R. White, and M. Eberl, "Pressure Filtration of Flocculated Suspensions," *AIChE J.*, **41**, 1687 (1995).

Miller, K. T., R. M. Melant, and C. F. Zukoski, "Comparison of the Compressive Yield Response of Aggregated Suspensions: Pressure Filtration, Centrifugation, and Osmotic Consolidation," *J. Amer. Ceram. Soc.*, **79**, 2545 (1996).

Perry, R. H., and D. W. Green, *Perry's Chemical Engineers' Handbook* 6th ed., McGraw-Hill, New York (1984).

Scherer, G. W., "Theory of Drying," *J. Amer. Ceram. Soc.*, **73**, 3 (1990).

Shepherd, C. B., C. Hadlock, and R. C. Brewer, "Drying Materials in Trays. Evaporation of Surface Moisture," *Ind. Eng. Chem.*, **30**, 388 (1938).

Sherwood, T. K., "The Drying of Solids: I," *Ind. Eng. Chem.*, **21**, 12 (1929).

Sherwood, T. K., "The Drying of Solids: II," *Ind. Eng. Chem.*, **21**, 976 (1929).

Sherwood, T. K., "The Drying of Solids: III," *Ind. Eng. Chem.*, **22**, 132 (1930).

Smith, D. M., G. W. Scherer, and J. M. Anderson, "Shrinkage During Drying of Silica Gel," *J. Non-Cryst. Solids*, **188**, 191 (1995).

Tiller, F. M., "Revision of Kynch Sedimentation Theory," *AIChE J.*, **27**, 823 (1981).

White, L. R., "Capillary Rise in Powders," *J. Colloid Interface Sci.*, **90**, 536 (1982).

Zuidema, H. H., and G. W. Waters, "Ring Method for the Determination of Interfacial Tension," *Ind. and Eng. Chem.*, **13**, 312 (1941).

Appendix A

Derivation of governing momentum balance equations

We take as our starting point the volume averaged equations for fully saturated two-phase flow of a solid/liquid system in the presence of a gravitational body force (Eqs. 1 and 2) viz

$$\frac{\partial \phi}{\partial t} + \nabla\cdot(\phi\vec{u}) = 0 \tag{A1a}$$

$$\frac{\partial (1-\phi)}{\partial t} + \nabla\cdot\left[(1-\phi)\vec{v}\right] = 0 \tag{A1b}$$

The conservation equations for incompressible phases where ϕ is the mean solids volume fraction and $\vec{u}$, $\vec{v}$ are the local mean velocities of the solid and liquid phases, together with the momentum conservation equations

$$\nabla\cdot\underline{\underline{\sigma}} - nf \rightharpoonup + (1-\phi)\rho_l\vec{g} = 0 \tag{A2a}$$

$$\nabla\cdot\sigma^s + nf \rightharpoonup + \phi\rho_s\vec{g} = 0 \tag{A2b}$$

We are neglecting in these equations inertial terms, and $\overline{\overline{\sigma}}^s$ is the contribution to the mean stress in the system supported by particle-particle interactions (solid-solid contact forces in the case of a flocculated solid network or intersurface colloidal forces in the case of a stable suspension). The mean fluid stress $\underline{\underline{\sigma}}$ acts throughout the total two-phase volume, not just in the fluid phase, but also inside the solid phase since the fluid stresses are transmitted to the solid phase via the solid-liquid interfaces where the local force balance must apply. We neglect here the Laplace pressure contribution to the interfacial force balance and, hence, to the mean stress inside the solid phase. The quantity $\vec{f}$ is the mean force on a solid particle exerted by the fluid phase, and n is the local mean number density of solid particles. We have that

$$\phi = nv_p \tag{A3}$$

where v_p is a mean particle volume. These volume averaged quantities change on a length scale L which is large compared to particle separations which are at least $\vartheta(a_p)$, where

a_p is the mean particle size. The shear components of $\nabla\cdot\underline{\sigma}$ are $\vartheta(\eta W/L^2)$, where η is the continuous phase viscosity and W is a typical fluid velocity change. The mean force $\vec{f}$ on a solid particle will contain (see below) a term which represents the local hydrodynamic drag on the particle and hence the $n\vec{f}$ term in the force balance equations is at least of $\vartheta\{[\eta\phi(u-v)]/a_p^2\}$. Provided that we are modeling a process where there is significant differential solid/liquid motion, that is, $(u-v)\approx\vartheta(W)$, we observe that the shear contribution to $\nabla\cdot\underline{\sigma}$ may be neglected in comparison to $n\vec{f}$. Hence, we may write

$$\underline{\sigma} = -P_l\underline{\underline{I}} \tag{A4}$$

where P_l is the mean hydrostatic pressure in the fluid phase.

The plastic rheological model (Buscall and White, 1987) that we invoke for the solid phase asserts that the solid network behaves as a solid, that is

$$\frac{D\phi}{Dt} = 0 \text{ for } |\underline{\underline{\sigma}}^2| < P_y[\phi(z,t)] \tag{A5}$$

and that, when $D\phi/Dt > 0$, fluid drainage is sufficiently rapid that the network can immediately adjust to make

$$\underline{\underline{\sigma}}^s = -P_y[\phi(z,t)]\underline{\underline{I}} \tag{A6}$$

Thus, the momentum equations (A2a, A2b) in this two-phase flow rheology may be written as

$$-\nabla P_l - n\vec{f} + (1-\phi)\rho_l g = 0 \tag{A7a}$$

$$-\nabla P_s + n\vec{f} + \phi\rho_s g = 0 \tag{A7b}$$

where the solids pressure P_s is given by

$$P_s(z,t) = P_y[\phi(z,t)] \tag{A8}$$

Adding Eqs. A7a and A7b gives

$$-\nabla(P_l + P_s) + [(1-\phi)\rho_l + \phi\rho_s]g \rightharpoonup = 0 \tag{A9}$$

which asserts that the total mean pressure at a point in the suspension is determined by the gravitational load of the slurry above that point. As discussed by Anderson and Jackson (1967), we may write

$$n\vec{f} = -\phi\nabla P_l + \frac{\lambda_{st}\phi r(\phi)}{v_p}(\vec{u}-\vec{v}) \tag{A10}$$

Substituting for $n\vec{f}$ in Eq. A7a yields

$$-(1-\phi)\nabla P_l + \frac{\lambda_{st}\phi r(\phi)}{v_p}(\vec{u}-\vec{v}) + (1-\phi)\rho_l g = 0 \tag{A11a}$$

$$-\nabla P_s - \phi\nabla P_l - \frac{\lambda_{st}\phi r(\phi)}{v_p}(\vec{u}-\vec{v}) + \phi\rho_s g = 0 \tag{A11b}$$

Dividing Eq. A11a by $(1-\phi)$ yields

$$-\nabla P_l + \frac{\lambda_{st}\phi r(\phi)}{v_p(1-\phi)}(u-v) + \rho_l g = 0 \tag{A12a}$$

and multiply this equation by ϕ and subtract from Eq. A11b yields

$$-\nabla P_s - \frac{\lambda_{st}\phi r(\rho)}{v_p(1-\phi)}(\vec{u}-\vec{n}) + \Delta\rho\phi g = 0 \tag{A12b}$$

where $\Delta\rho = \rho_s + \rho_l$.
Identifying

$$R(\phi) = \frac{\lambda_{st}a_p^2}{\eta v_p}\phi r(\phi) \tag{A13}$$

and setting $\vec{g} = 0$, we obtain Eqs. 1 and 2.

Appendix B

Using the previously defined variables, we can rewrite Eq. 38 as

$$\frac{\partial(f\theta)}{\partial T} = \epsilon\frac{\partial}{\partial w}\left(k\phi\frac{\partial\theta}{\partial w}\right) - \phi\frac{\partial}{\partial w}[(\alpha+\beta)\theta] - \delta\frac{\partial(f\theta)}{\partial w} \tag{B1}$$

where

$$\epsilon = \frac{\phi}{\phi_0^2 D(\phi_0)} \tag{B2}$$

$$\alpha = \rho_l C_{pl}\left(-\overline{Q} + \epsilon\frac{D(\phi)}{(1-\phi)}\frac{\partial\phi}{\partial w}\right) \tag{B3}$$

$$\beta = \rho_s C_{ps}\left(-\overline{Q} - \epsilon\frac{D(\phi)}{\phi}\frac{\partial\phi}{\partial W}\right) \tag{B4}$$

$$\delta = \epsilon D(\phi)\frac{\partial\phi}{\partial w} + \phi\overline{Q} \tag{B5}$$

$$f = [\phi\rho_s + (1-\phi)\rho_l][\phi C_{ps} + (1-\phi)C_{pl}] \tag{B6}$$

where Eq. B1 has the initial condition

$$\theta(w,0) = \theta_0 \tag{B7}$$

and boundary conditions

$$-k\frac{\phi}{\phi_0 h_0}\frac{\partial\theta}{\partial w}\bigg|_{(0,T)} = h_c[\theta_g - \theta(0,T)] - \frac{\phi_0 D(\phi_0)\overline{Q}}{h_0}\lambda_v\rho_l \tag{B8}$$

$$\frac{\partial\theta}{\partial w}\bigg|_{(1,T)} = 0 \tag{B9}$$

Manuscript received Dec. 15, 2000, and revision received Aug. 8, 2001.